



OPEN Experimental investigation on the effect of solid particle erosion on the water droplet erosion damages for blade materials

Juan Di^{1,2,3}✉, Jun Ji¹, Jin Xu¹, Zhi Li¹, Ke Ning⁴, Chao-yi Peng^{2,3} & Jian-feng Wang³

In this paper, the influence of solid particle erosion on the water droplet erosion is explored based on the self-developed erosion test system and high-speed rotating waterjet test rig. The results show that the WDE morphology exhibited distinct structural divergence: substrates displayed stepped fibrous textures (10–20 μm), while the surface presented honeycomb-like stalactite peak cluster structure with each stalactite petal about 2 μm , which is close to the natural stalactite morphology. Besides, it is found that the regular texture or mesh structure of the machined surface is more conducive to the diversion and expansion of the liquid flow than that of the uneven and irregular structure surface formed by the solid particle erosion, making more serious erosion damage of the latter. For martensite substrate and stellite cladding materials, the differences are 5.87 and 2.52 times, respectively.

Keywords Solid particle erosion, Water droplet erosion, Surface microstructure, Blade materials, WDE microstructure

Solid particle erosion (SPE) and water droplet erosion (WDE) represent two predominant degradation mechanisms threatening the integrity of turbine blades. SPE arises from high-velocity impingement of micro-particles (e.g., oxide spallations from boiler tubes) causing surface pitting and roughness escalation. WDE initiates from repetitive droplet impacts in wet steam zones¹. The last stage blades of thermal power and nuclear power condensing steam turbines particularly suffer from severe WDE damage due to prolonged exposure to wet-steam zones. This degradation deteriorates aerodynamic efficiency and elevates safety risks in modern turbines employing lengthened blades with tip velocities exceeding 600 m/s². Field evidence from power plants in China confirms this dual erosion mechanism. Each low-pressure cylinder accumulates up to 40 kg of oxide particles (Panshan plant) and severe SPE pitting occurs on low-pressure blades (Haimen plant), indicating the coexistence of SPE and WDE risks in actual operations of low-pressure blades, as shown in Fig. 1. This indicates that the entrained ferric oxides and impurities peeled from boiler superheater/reheater tubes within wet-steam flow contribute to secondary SPE damage in low-pressure cascades³.

Recent research and microscopic observations have shown that WDE performance is highly sensitive to the regularity of surface structure^{4–6}. And the effect of SPE will produce a large number of random pits on the surface of the material to form a special irregular surface structure. Therefore, the influence of the fine particles should be considered when studying the water droplet erosion process of the last stage blade substrates and surface strengthening layers^{7,8}.

Studies by Mahdipoor et al.⁹, Mann et al.¹⁰, and Ahmad et al.¹¹ demonstrated that initiation and expansion of crack initiates via stress waves and lateral jetting from droplet impacts, with pre-existing surface irregularities amplifying the damage. Concurrently, Scholars mainly focus on the theoretical model^{12–16}, main influencing factors¹⁷, numerical methods¹⁸ and protective measures^{19,20} to study SPE behavior. Besides, the main failure mechanisms of SPE for plastic target are micro-cutting and extrusion-forging, or micro-ploughing and extrusion-forging corresponding to flaky or spherical particles, respectively²¹. SPE could may theoretically accelerate WDE progression through surface morphology modifications. However, conventional erosion models exclude this coupling effect, relying on the outdated premise of mutually exclusive particle and droplet impingement on

¹School of Vehicle and Transportation Engineering, Taiyuan University of Science and Technology, Taiyuan 030024, China. ²Zhuzhou Times New Material Technology Co., Ltd., Zhuzhou 412007, China. ³College of Materials Science and Engineering, Hunan University, Changsha 410082, China. ⁴Engineering Research Center Heavy Machinery Ministry of Education, Taiyuan University of Science and Technology, Taiyuan 030024, China. ✉email: juandi@tyust.edu.cn; dijuan.2008@163.com

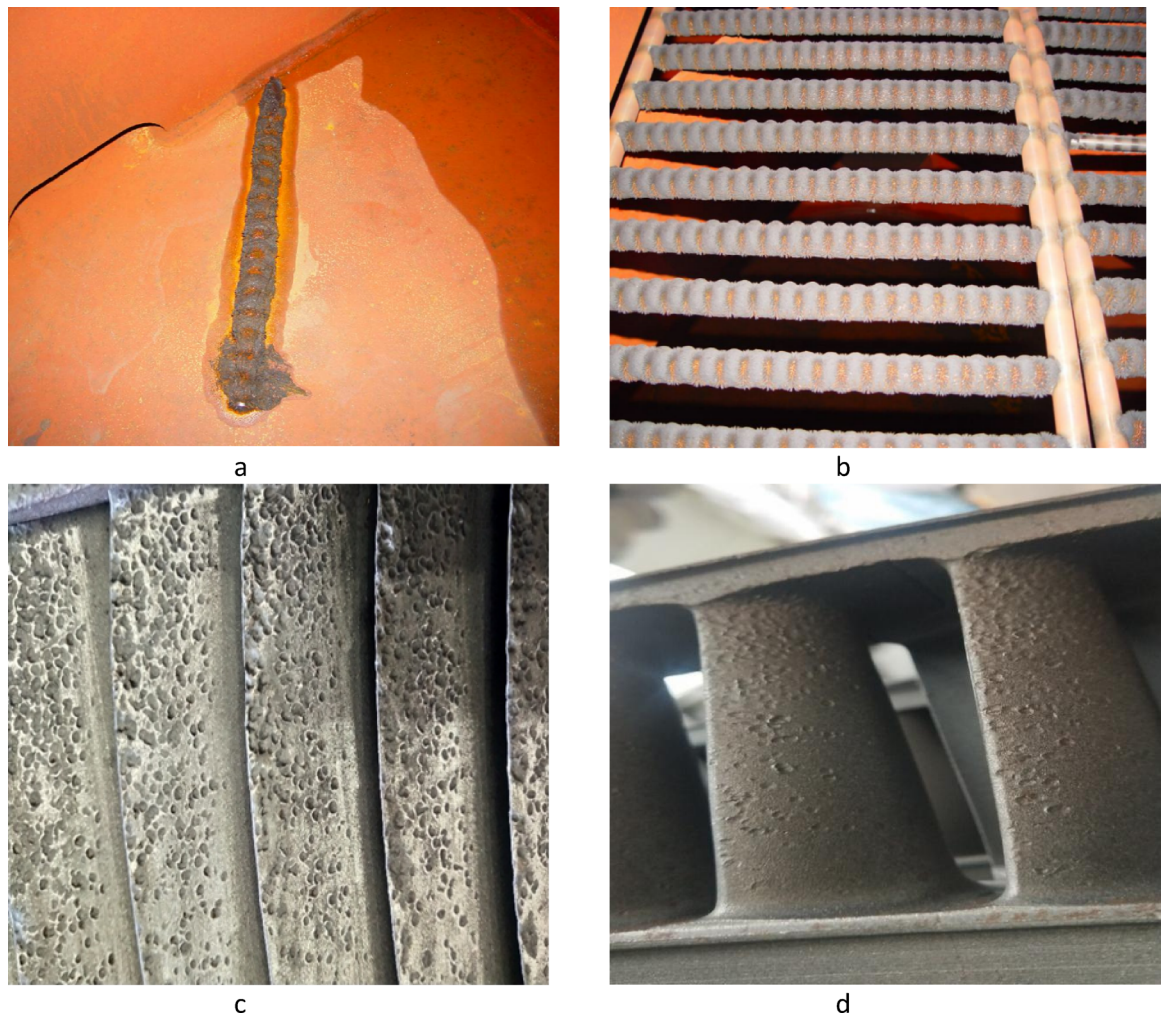


Fig. 1. The SPE damage morphologies in the blades of low pressure stage. (a) Oxide particles adsorption on the single condenser; (b) Oxide particles adsorption on several condensers; (c) Serious SPE damage of the first stage rotor blade in the low pressure cylinder (d) Serious SPE damage of the first stage stator blade in the low pressure cylinder.

blades. While surface roughness effects on WDE have been explored^{1,5}, no systematic study quantifies how SPE-induced microstructures modulate subsequent WDE behavior^{7,11}. The synergistic interaction of SPE and WDE on low-pressure blades exacerbates material degradation through coupled mechanical impacts, creating complex failure pathways validated by on-site situation. Current research remains fragmented, isolating these erosion mechanisms rather than addressing their interdependence—a critical knowledge gap for turbine reliability optimization in wet-steam environments.

On the basis of erosion rate, particle concentration measurements (0.001 mg/kg steam) by a typical erosion nozzle, support this dilute-phase premise (the particles within 0.1 kg/m^3 as dilute phase)^{22,23}. Therefore, the solid particles in the actual turbine cascade are dilute phase. The particles and water droplets simultaneously impinge on the blade surface is almost impossible. The sequential SPE-WDE interactions occur during the operational condition. With increase of last stage blade length, the maximum circumferential velocity on the tip of the blade has exceeded 600 m/s^2 . And the velocity of solid particles hitting the cascade is within the range of 150 to 360 m/s ^{24–26}.

Therefore, in this paper, a sequential SPE-WDE test was carried out using an upgraded SPE rig and high-speed rotating waterjet test platform to investigate the effect of SPE-generated surface microstructure induced by micro-particles impact on WDE progression for blade substrate and surface strengthening layers. The typical impact velocity of 200 m/s for solid particles and 650 m/s for water droplets were selected in our SPE tests and WDE tests. By correlating surface microstructure evolution with cumulative erosion weight loss, this work provides the mechanism framework and data foundation for SPE-WDE synergy in steam turbine blades under actual operating conditions, offering critical insights for novel erosion-resistant blade design.

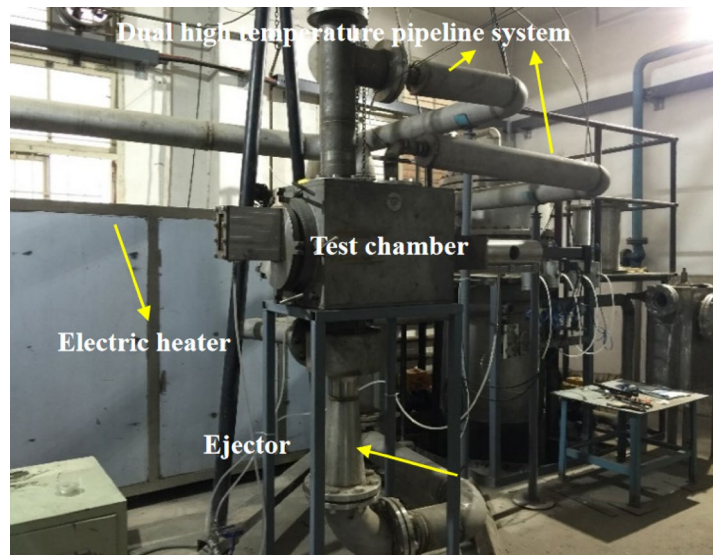
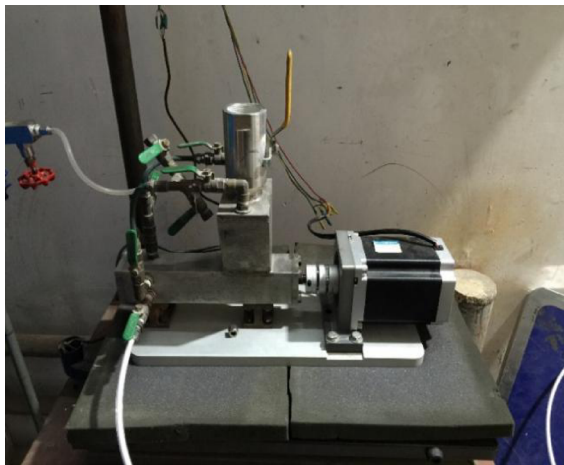


Fig. 2. The physical diagram of the SPE test system.



a. Screw feeding system



b. The clamping apparatus with different angles

Fig. 3. The critical components of SPE test system.

Experimental procedures

Figure 2 presents the physical diagram of the SPE test system, which is mainly composed of the erosion test chamber, gas source system, particle feeding system and exhaust system. The brief introduction is presented in²¹. The working process of this test system is as follows:

The primary airflow enters a long acceleration nozzle, where the particles produced by the screw feeder (Fig. 3a) are transported to the throat of the nozzle and accelerated to a specified speed. Particle feed rates are controlled via a stepper motor-driven system, ensuring precise gas–solid flow generation prior to target impingement in the test chamber. Post-impact particulates are evacuated through an ejector-cyclone separation system for continuous operation. Four 17-4PH stainless steel specimens are directly mounted on a servo-actuated T-groove fixture (Fig. 3b), enabling automated positional switching during testing. As fixture replacement necessitates recalibration of the air pressure and stepper motor speed for the feeding system, the outermost specimen (Position 1) serves as a pre-test calibration sample with subsequent data exclusion to guarantee the reliability of subsequent test results. Additionally, the integrated electric heater (max 800 °C ± 15 °C) facilitates thermal state SPE experiments.

Schematic diagram of WDE test platform is shown in Fig. 4 (created by SOLIDWORKS 2018, <https://www.solidworks.com>). The system is mainly composed of ultra-high pressure pump (240–260 MPa), test chamber with impeller-mounted specimens connected to the rotating shaft (rotational speed controlled by the cabinet and the 1:3 gear speed increaser), lubrication system, and drainage system. As shown in Fig. 4, a waterjet with

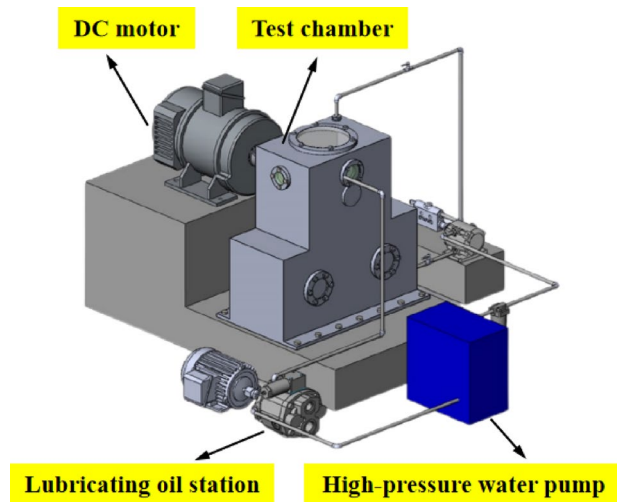


Fig. 4. Schematic diagram of WDE test platform.

Parameters	Vacuum pressure (kPa)	Nozzle pressure (MPa)	Nozzle diameter (mm)	Waterjet velocity (m/s)
Values	14	242	0.15	650

Table 1. The test parameters of the WDE in the test.

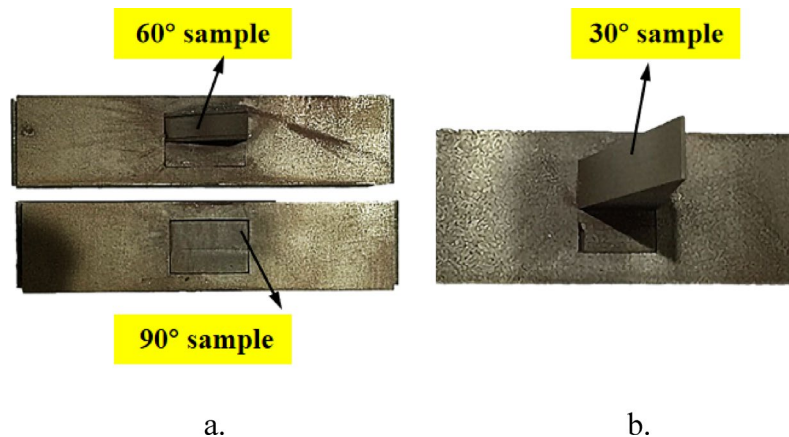


Fig. 5. The samples after 2 min SPE test. (a) Martensite substrate samples after 2 min SPE test (the top is 60° sample and the bottom is 90° sample); (b) 30° sample of the stellite laser cladding material after 2 min SPE test.

the maximum velocity of 650 m/s is generated by a nozzle embedded with diamond (\varnothing 0.15 mm). The detailed description of the test system could be seen in references^{4,27}.

Experimental sequence: a. SPE test: The martensitic substrates and stellite laser cladding specimens were subjected to iron oxide particle impacts (Sauter Mean Diameter \approx 100 μm)²¹ at 200 m/s for various impact angles (15°–90°) and durations (1–5 min). b. WDE test: Subsequent testing employed a diamond-embedded nozzle with diameter of 0.15 mm generating 650 m/s waterjet (mass flow rate: 0.0115 kg/s with a rough estimation) for 90-min exposure period. The detailed test parameters of WDE are presented in Table 1.

In order to study the effect of impact angles on the WDE characteristics, a stepped structure of specimen is designed (Fig. 5). Figure 5a depicts the martensite substrate sample after 2 min SPE test, with the top featuring a 60° sample and the bottom a 90° sample. Figure 5b shows the 30° stellite laser cladding sample after 2 min SPE test.

The specific test scheme is shown in Table 2. Table 3 lists the chemical composition and mechanical properties of martensite substrate and the stellite laser cladding materials.

The installation of the specimen on the impeller turntable of high-speed waterjet test system is shown in Fig. 6a. Figure 6b displays the real-time image captured during the water droplet erosion test. The target samples

Material	SPE time	SPE angle	WDE time	WDE angle
17-4PH	1–5 min	60°, 90°	90 min	60°, 90°
Stellite laser cladding	1–5 min	30°, 60°, 90°	90 min	30°, 60°, 90°

Table 2. SPE test scheme.

	17-4PH	Stellite laser cladding
Composition (wt%)	16.2Cr, <0.07C, 3.7Ni, 3.5Cu, 0.2Nb, 0.4Si, 0.2Mo, 0.5Mn, bal.Fe	28Cr, 4W, 3Ni, 2Si, 1.2C, bal.Co
Density (g/cm ³)	7.861	8.9
Poisson ratio	0.29	0.282
Elastic modulus (GPa)	196.5	212
Yield strength (MPa)	724	1071
Tensile strength (MPa)	931	1414
Vickers hardness (HV)	330–350	440

Table 3. Chemical composition and mechanical properties of blade materials.

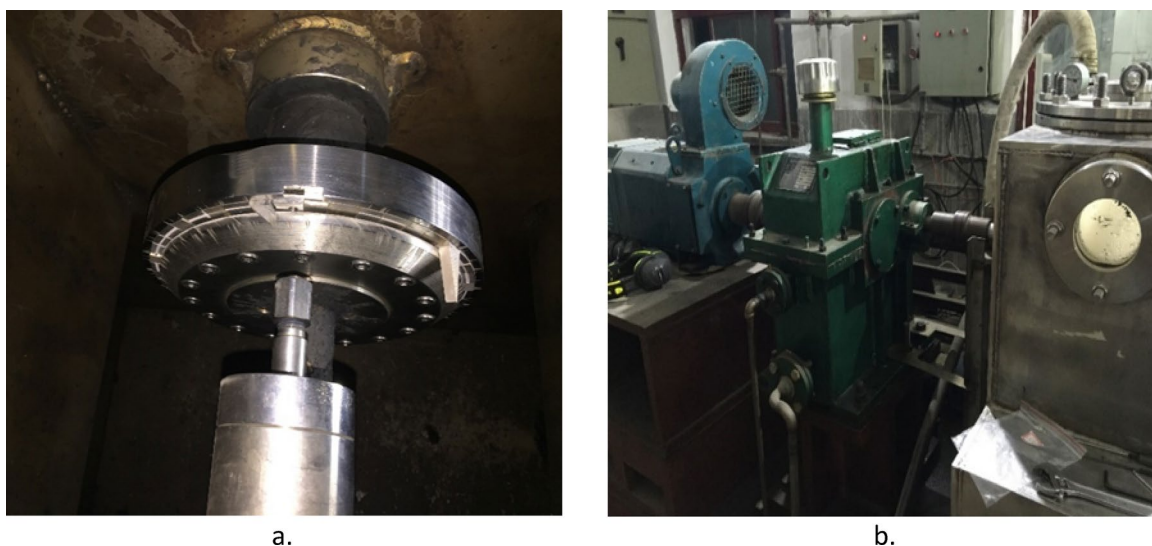


Fig. 6. The high-speed waterjet test rig. (a) The installation of the specimen on the impeller turntable; (b) The real-time image during the WDE test.

after ultrasonic cleaning with anhydrous ethanol for 5 min and drying after SPE tests and 90 min WDE tests are presented in Fig. 7a and b, respectively.

Results and discussions

WDE mass loss and damage caused by SPE

Post-WDE mass loss quantification at 10-min, 30-min, and 90-min intervals revealed distinct erosion characteristics for substrates and cladding specimens, as shown in Fig. 8. 90° samples only by WDE test were used as the control group and labeled as 90°-WDE. The results indicate that the cumulative WDE mass loss of the substrate control group is about average 15 times than that of the cladding sample, which proved that the WDE resistance of the stellite cladding sample was far better than that of the martensite substrate.

Substrate erosion rates increased exponentially with SPE exposure time for 1 min, 2 min, 3 min, and 5 min (0.308 mg/min → 0.317 mg/min → 0.324 mg/min → 0.334 mg/min at 90°). The 90°-WDE control group exhibited stable erosion rates (0.056 mg/min), approximately 17.47% of the mass loss rates observed in all 90° samples subjected to solid particle erosion. while SPE-pretreated samples demonstrated angle- and duration-dependent WDE damage acceleration.

For the stellite cladding samples exposed to solid particle erosion, the cumulative WDE mass loss rates during the initial 10 min WDE test, were 0.02 mg/min, 0.03 mg/min, 0.05 mg/min, 0.07 mg/min, and 0.09 mg/min, respectively. Subsequent 20-min and the final 60-min exposure showed approximately 75.92% and 88.34% reductions in mass loss rates, respectively, contrasting with the minimal rate of the control group (0.0033 mg/min), which was significantly lower than all SPE-treated samples.

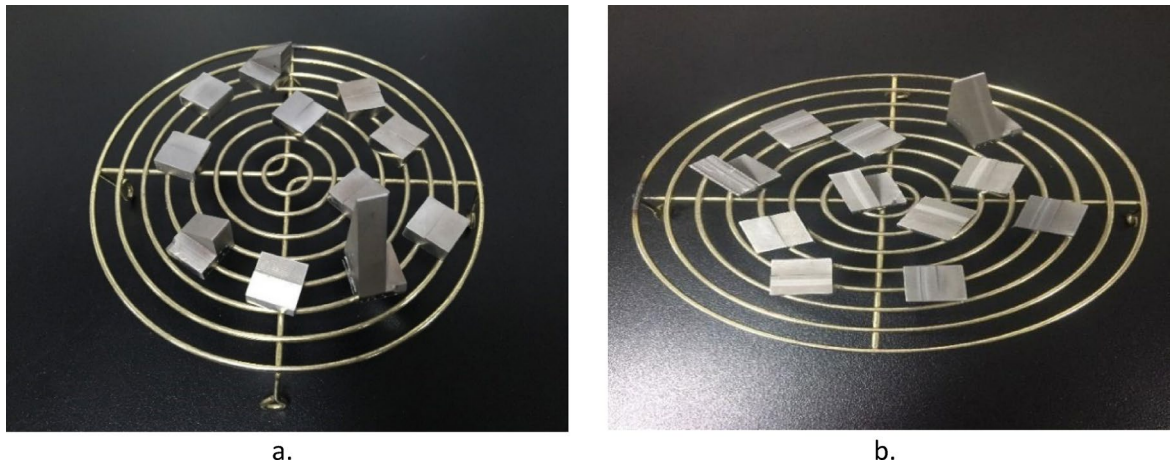


Fig. 7. The target samples after ultrasonic cleaning and drying. (a) The target samples after ultrasonic cleaning and drying after the SPE tests; (b) The target samples after ultrasonic cleaning and drying after 90 min WDE tests.

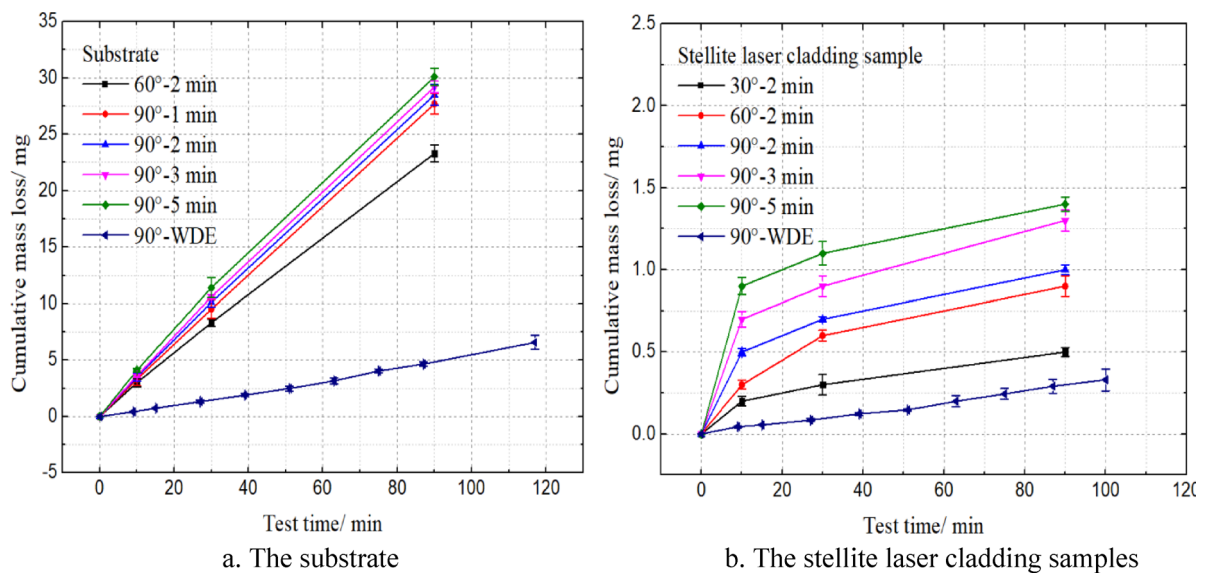


Fig. 8. The variation of mass loss of the substrate and the stellite laser cladding samples along the testing time.

In conclusion, increasing the impact angles and test duration of SPE significantly exacerbate WDE damage. Within the duration of this experiment, the effect of solid particle erosion on WDE rate of cladding samples notably weakens with the increasing WDE duration, while the erosion rate of substrate samples remains relatively constant, and the influence of WDE duration can be ignored.

The clearly visible deep groove was formed on the surface of 17-4PH substrate samples, while only a white trace zone was formed in the WDE region, as shown in Fig. 9. In contrast, only an etched trace band with a width of about 430 μm with an extremely thin hair-like trace groove in the center was observed under the scanning electron microscope (SEM) after 90-min WDE test due to the slow progression of WDE damage for cladding samples, under SEM. The depth of the groove was very shallow and almost negligible, as shown in Fig. 10.

Figure 11 shows the distribution of the width and depth of the erosion zone of the substrate along testing time. The 17-4PH substrate exhibited obvious visible surface delamination (122–156.6 μm width, 72.1–114.3 μm depth) after 10-min WDE exposure, progressing to catastrophic erosion (813.5–901.6 μm width, 262.7–307.9 μm depth post-90-min) due to lateral flow constraints concentrating impact forces. It can be seen that the erosion width and depth of the substrate increased with the increasing erosion time. In addition, as the water erosion time increased, the growth rate of erosion width of the substrate decreased with the test time. And the growth rate of erosion depth gradually increased with test time. This is because in the initial stage, the waterjet can be freely expanded, so the width expansion was relatively easy. As the erosion continued, the water column impacted in the WDE groove, and will be subjected to a larger lateral constraint, making the impact force more concentrated. So the width expansion becomes slow, and the depth expansion speeds up.

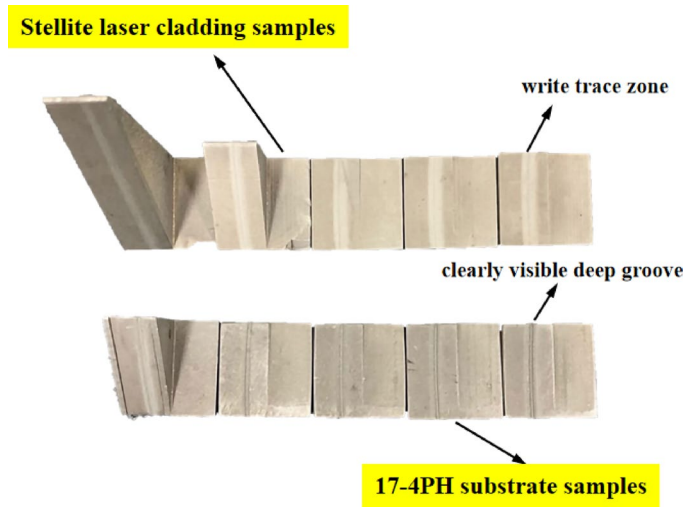


Fig. 9. The surface damage marks of the substrates and the stellite laser cladding samples.

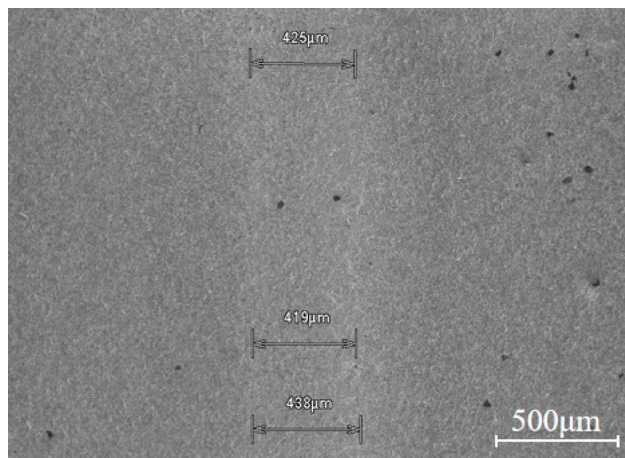


Fig. 10. A water-etched trace band after 90 min WDE test for the stellite cladding sample.

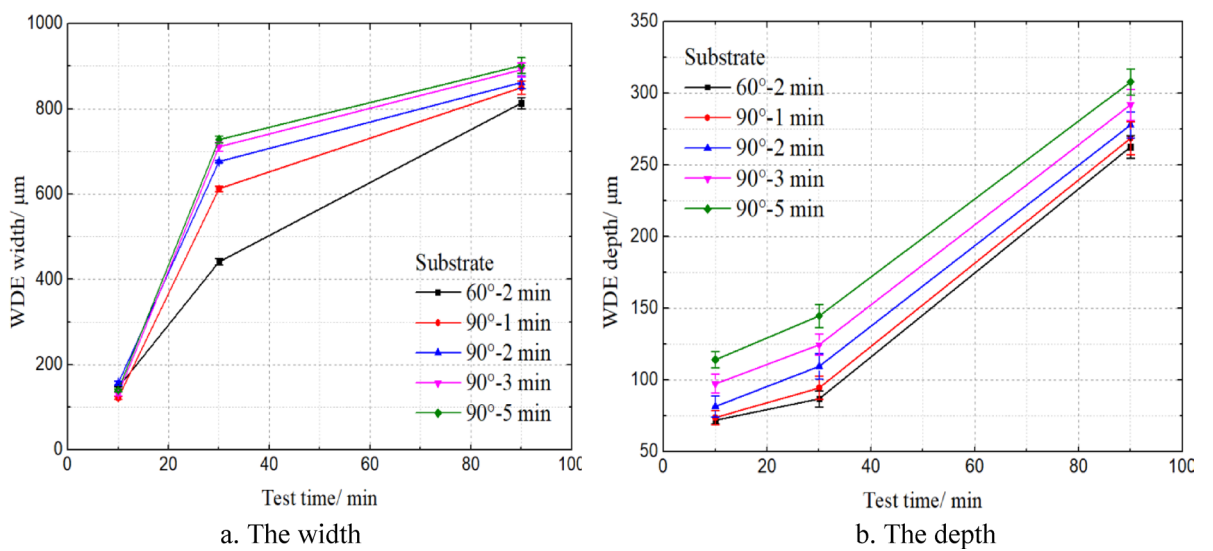


Fig. 11. The distribution of the width and depth of the erosion zone of the substrate along testing time.

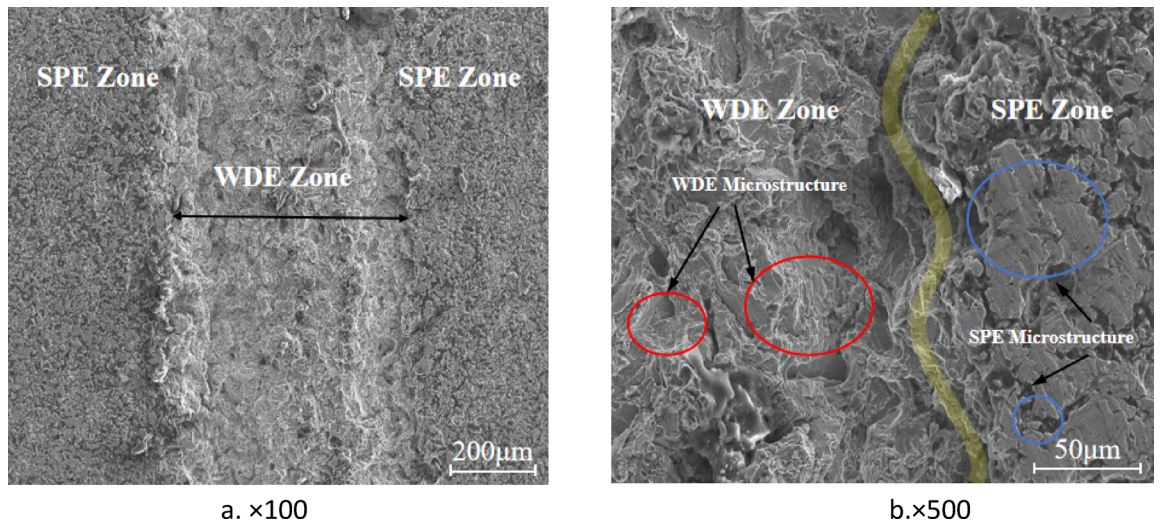


Fig. 12. The micro morphology WDE and SPE of the martensite substrate after 5 min SPE and 10 min WDE. (a) $\times 100$; (b) $\times 500$.

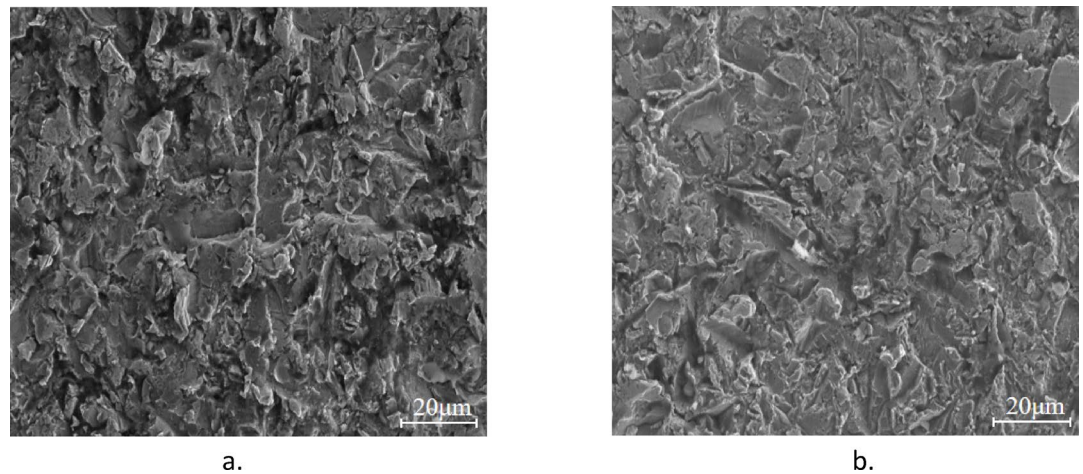


Fig. 13. SPE morphologies of the martensite substrate and the stellite cladding sample. (a) Substrate; (b) Stellite laser cladding sample.

The typical microscopic morphology of SPE and WDE

The micro WDE and SPE morphology of the martensite substrate after 5 min SPE and 10 min WDE are shown in Fig. 12. It can be seen from the figures that there is an obvious difference in the microscopic morphology of the SPE and WDE zone for the substrate samples. The SPE zone has a typical plate-like structure. And there are many cutting scratches, grooves and lips disorderly distributed on the surface. And the WDE region is a multi-fibrous terracing step-shaped structure with river-like patterns. It can be seen from Fig. 13 that the SPE morphologies of the martensite substrate and the stellite cladding sample are basically similar both with typical lamellar morphology. The microscopic morphology of the stellite laser cladding specimen after 5 min SPE and 10 min WDE is shown in Fig. 14. It can be seen that the surface of the stellite laser cladding sample exhibits a very obvious plate-like SPE morphology. While the water droplet erosion marks are still almost invisible.

The morphologies of the stellite laser cladding sample and the martensite substrate after 30 min WDE test are shown in Fig. 15 (2 min SPE) and Fig. 16 (5 min SPE), respectively. The obvious damage morphology formed in the WDE zone of the stellite cladding specimen.

In addition, it can be clearly seen from the figures that there is a significant difference in the micro structure of the WDE region for the substrate and the stellite cladding samples. The WDE area of the substrate sample has a very pronounced stepped fibrous structure. While the micro morphology of the stellite cladding sample presents a honeycomb stalactite peak cluster structure which is similar to the natural stalactite morphology. The formation process of the natural stalactite morphology usually takes thousands or millions of years. Due to such a lengthy forming process, it is speculated further that such a microstructure is probably the underlying reason for the superior WDE resistance of the stellite laser cladding sample.

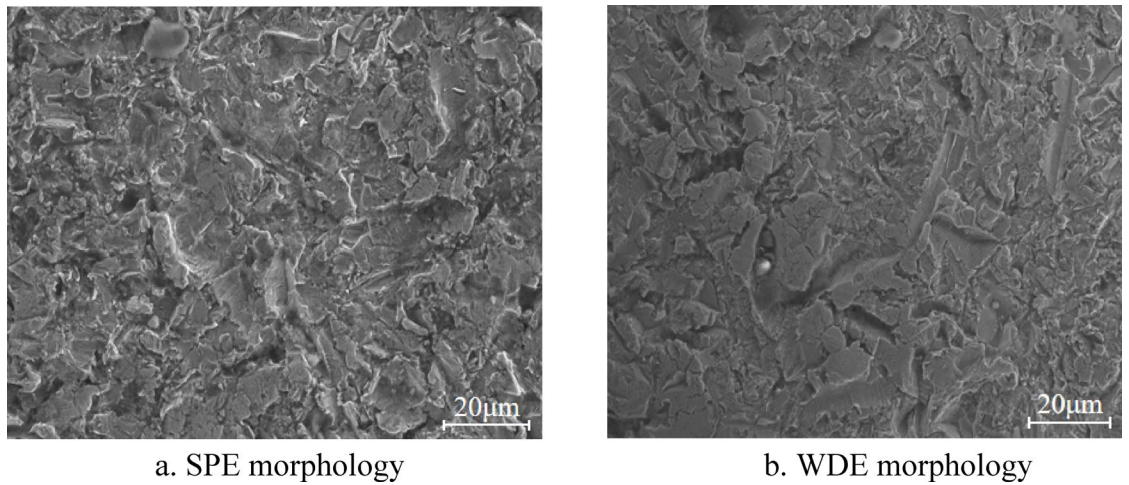


Fig. 14. The microscopic plate-like SPE morphology and WDE morphology of the stellite laser cladding specimen after 5 min SPE and 10 min WDE.

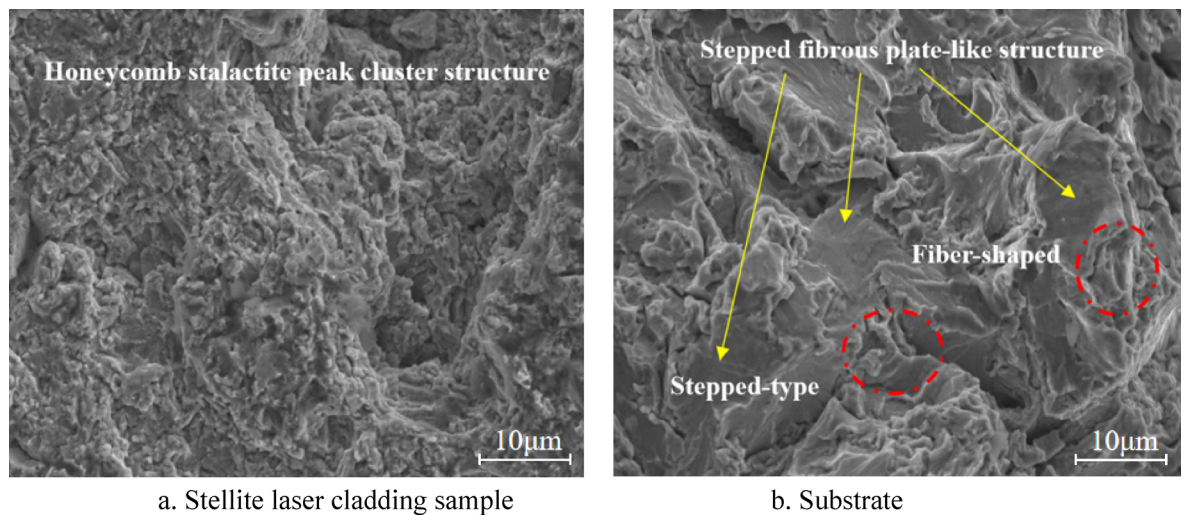


Fig. 15. The WDE morphologies of the stellite laser cladding sample and the martensite substrate after 30 min WDE test (2 min SPE + 30 min WDE).

Besides, the size of WDE microstructures of the two materials is also worth emphasizing. The size of each stalactite-like petal in WDE zone of the stellite cladding samples is about 2 microns, while the stepped structure of martensite substrate is obvious larger within the range of 10–20 microns.

The microscopic morphologies of the two kinds of materials after 2 min SPE and 90 min WDE test are shown in Fig. 17. It is obvious that the microstructures in the WDE zone for the two materials are more distinct.

The quantitative analysis of WDE damage by SPE-induced surface microstructure

The variation of cumulative mass loss curve along erosion time of wire cutting 17-4PH and stellite laser cladding sample for only conventional WDE test is shown in Fig. 18. The corresponding data are used as the control group, as shown in Tables 4 and 7.

The effect of solid particle erosion on WDE damage behaviour for 17-4PH substrate was analysed base on the 30 min test data. It can be seen from Tables 4 and 5 that the solid particle erosion of micro particles had a significant influence on the WDE damage characteristics of the blade substrate, which accelerated WDE damage of the wire cutting 17-4PH substrate samples by about 5.87 times. The WDE damage surfaces of 17-4PH with prior SPE and without SPE under 30 min and 155 min WDE test are presented in Fig. 19, respectively. The eroded average width and corresponding mass loss of WDE zone was 704 μm /9.5 mg and 760 μm /8.7 mg, respectively. The results also provided powerful support for the fact that SPE could lead to more severe WDE damage.

The surface roughness of the samples measured by portable surface roughometer TIME 3100. It was found that the roughness after SPE only increased by 0.0445–0.1295 μm by measuring the surface roughness before and after solid particle erosion. The average variation was 5.67%, as shown in Table 6. From the above results,

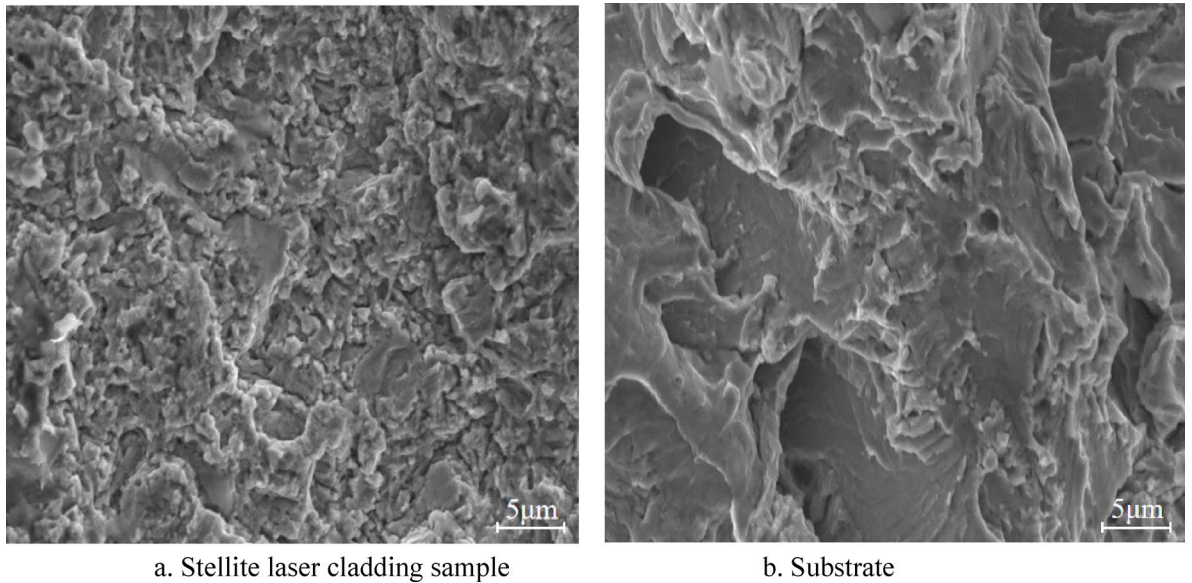


Fig. 16. The WDE morphologies of the stellite laser cladding sample and the martensite substrate after 30 min WDE test (5 min SPE + 30 min WDE).

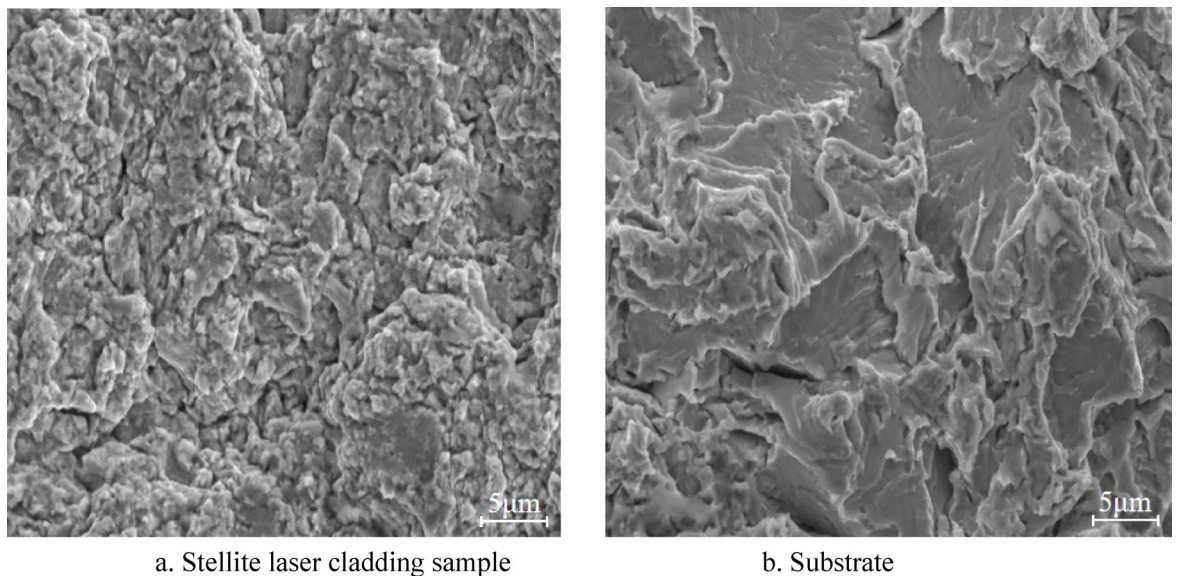


Fig. 17. The microscopic morphologies of the stellite laser cladding specimen and the martensite substrate after 2 min SPE and 90 min WDE test.

it was indicated that such a little change in surface roughness before and after SPE still significantly aggravated the WDE damage.

Furthermore, the surface morphologies of the samples were studied by microscope observation. It was worth noticing that the microstructures were significantly different between the wire cutting and SPE samples under SEM observation. The surface of the conventional wire cutting specimen had a regular metal texture or mesh structure (see Fig. 20a). While the target surface after SPE formed an intricate irregular morphology. Various grooves, accumulated lips and scratches were randomly distributed on the surface as shown in Fig. 20b.

Hence, it can be speculated that the orderly texture or grid pattern created on the machined surface facilitates the diversion and dispersion of liquid flow, resulting in relatively minor damage. Conversely, the irregular surface structure induced by SPE impedes the unhindered expansion of liquid flow, significantly reducing the latency period of water droplet erosion, thereby leading to more severe WDE damage. The above studies fully demonstrate that the significant effect of solid particle erosion on the acceleration of WDE damage of the substrate is mainly determined by the surface microstructure.

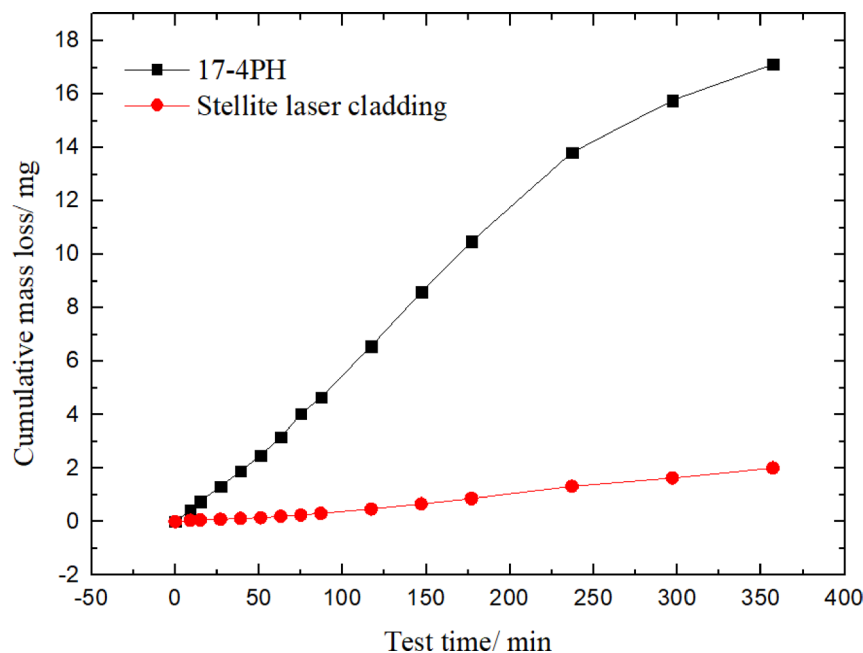


Fig. 18. The variation of cumulative mass loss curve along testing time of wire cutting 17-4PH and stellite laser cladding sample along erosion time for the conventional WDE test.

WDE test time/min	Mass loss of wire-cut substrate/mg
147	8.59
177	10.49
237	13.82
297	15.77

Table 4. Statistical table of mass loss for conventional WDE test of wire-cut 17-4PH substrate samples.

Substrate	Mass loss after 30 min/mg	Corresponding to the common WDE minutes (Interpolation method)	Multiple relationship
90°-1 min	9.5	161.37	5.379
90°-2 min	10.1	170.84	5.695
90°-3 min	10.6	178.98	5.966
90°-5 min	11.4	193.40	6.447
Average multiple: 5.87			

Table 5. Statistical table of mass loss of martensite 17-4PH substrate samples exposed to SPE.

Similarly, the influence of solid particle erosion on the water droplet erosion performance of the stellite cladding sample is studied. It is also found that the solid particle erosion has a significant effect on the WDE damage. The solid particle erosion accelerates by an average of about 2.52 times WDE damage compared with the conventional wire cutting stellite laser cladding sample. The detailed data are shown in Tables 7 and 8.

The WDE damage surfaces of stellite laser cladding samples with prior SPE and without SPE under 90 min WDE test is presented in Fig. 21, respectively. The average mass loss of WDE zone is 1.0 mg and 0.4 mg, respectively. The visible damage morphologies and mass loss of the samples with prior SPE are significantly more severe than those without SPE in the same 90 min WDE test, which fully indicated that SPE damaged surface greatly accelerated the water droplet erosion rate.

It is found that the surface roughness after SPE increases 0.0425–0.318 μm compared with the wire-cut ones. The average variation is 19.35%, as shown in Table 9. Likewise, the WDE damage of cladding material is also aggravated by SPE despite of the little change of the surface roughness.

Microstructural analysis reveals conventional wire cutting specimen exhibits a regular metal texture or mesh structure, while the surface after SPE is in wild disorder as shown in Fig. 22. The above studies show that the water droplet erosion performance is particularly sensitive to the surface structure. Namely, the solid particle erosion accelerates the water droplet erosion damage of the blade substrate and the strengthened stellite laser

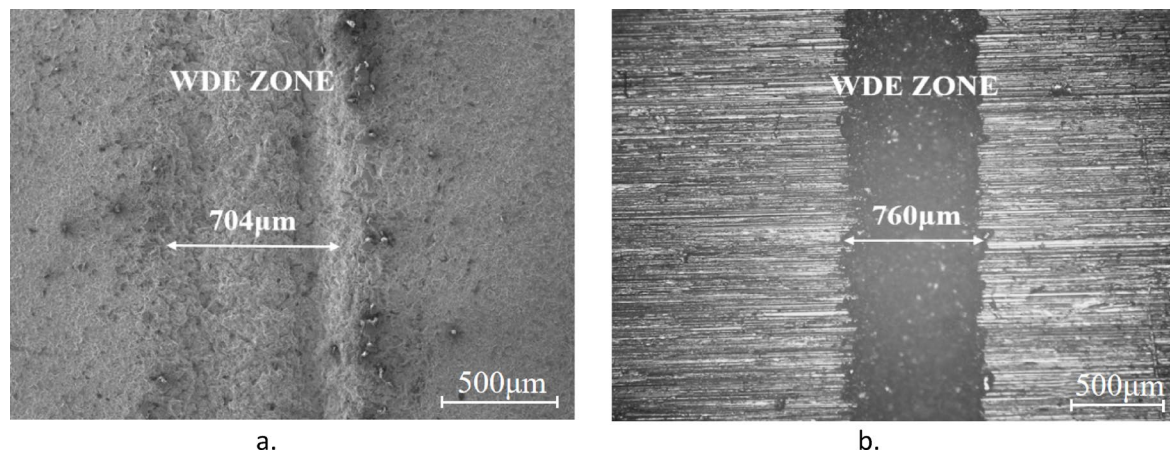


Fig. 19. The WDE damage surfaces of 17-4PH with prior SPE and without SPE under 30 min and 155 min WDE test. **(a)** 30 min WDE with prior SPE corresponding mass loss: 9.5 mg; **(b)** 155 min WDE without SPE corresponding mass loss: 8.7 mg.

Surface roughness before SPE/ μm	Surface roughness after SPE/ μm	Roughness relative variation
1.453	1.5825	8.9%
1.39	1.46	5.04%
1.448	1.4925	3.07%
Average variation: 5.67%		

Table 6. Statistical table of surface roughness before and after SPE for the wire-cut substrate samples.

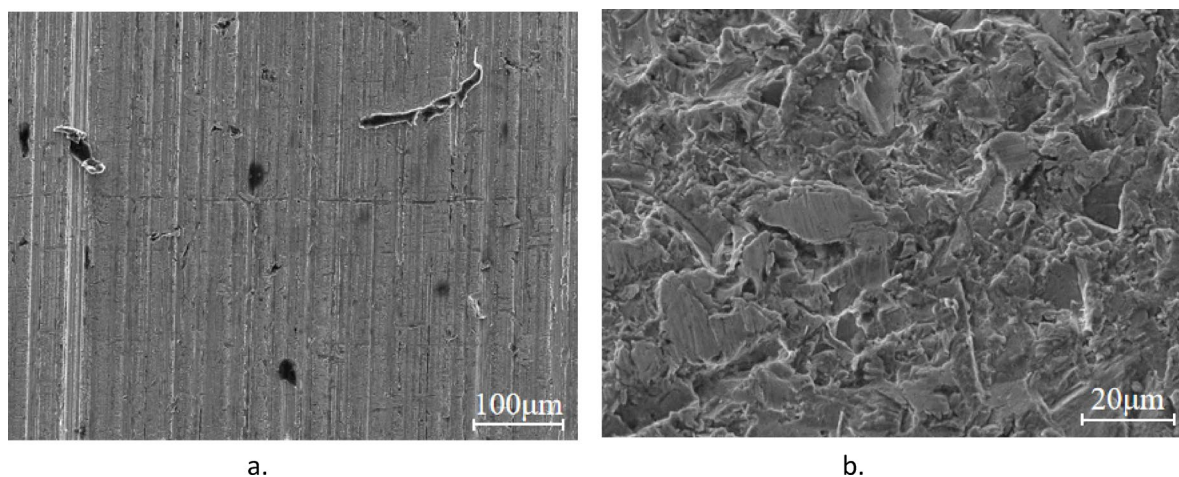


Fig. 20. Surface microscopic morphology of martensite substrates. **(a)** Surface morphology of the wire-cut 17-4PH substrate sample; **(b)** Surface morphology with SPE.

cladding material, which is mainly determined by the surface irregular structure. The irregular and uneven microstructure of surface formed by SPE is not conducive to the drainage and expansion of the liquid flow, resulting in greatly shortening the latency and accelerating the erosion damage.

Conclusions

This study investigates the synergistic effects of solid particle erosion (SPE) on water droplet erosion (WDE) performance through a self-developed SPE test system and the high-speed rotating waterjet test platform. Key findings are summarized as follows:

1. SPE generates irregular surface structures that shorten WDE latency and accelerate damage progression. Regular machined textures is more conducive to the drainage and expansion of the liquid flow than that of

WDE test time	Mass loss/mg
177	0.867
237	1.32
297	1.63
357	2.01

Table 7. Statistical table of mass loss for conventional WDE test of the wire-cut cladding samples.

Cladding sample	Mass loss of 90 min/mg	Corresponding to the common WDE minutes (Interpolation method)	Multiple relationship
90°-2 min	1.0	194.616	2.16
90°-3 min	1.3	234.351	2.6
90°-5 min	1.4	252.484	2.81
Average multiple: 2.52			

Table 8. Statistical table of mass loss of cladding sample exposed to SPE.

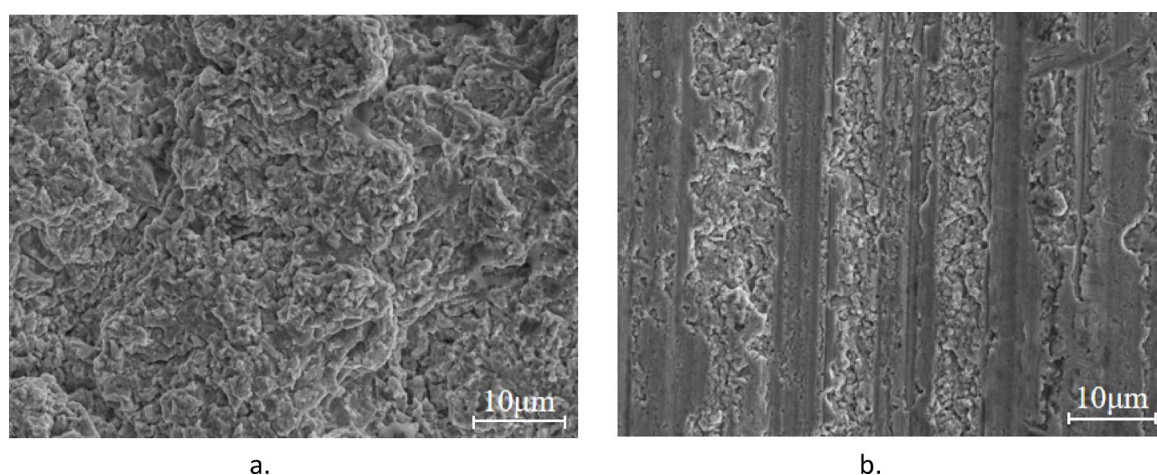


Fig. 21. The WDE damage surfaces of stellite laser cladding samples with prior SPE and without SPE under 90 min WDE test. (a) 90 min WDE with prior SPE corresponding mass loss: 1.0 mg; (b) 90 min WDE without SPE corresponding mass loss: 0.4 mg.

Surface roughness before SPE/ μm	Surface roughness after SPE/ μm	Roughness relative variation
1.19	1.2325	3.57%
1.042	1.36	30.52%
1.022	1.2725	24.51%
Average variation: 19.53%		

Table 9. Statistical table of surface roughness before and after SPE of the wire-cut cladding samples.

- the irregular structure surface formed by the solid particle erosion, which makes more serious WDE damage of the latter.
2. Solid particle erosion significantly affects the water droplet erosion performance of 17-4PH substrate and the Stellite laser cladding samples, accelerating WDE damage by 5.87 times and 2.52 times, respectively.
 3. It is worth noting that the SPE microstructure of the blade substrate is similar to the stellite cladding sample in the SEM observation. But the WDE morphology is significantly different. a. WDE morphology for Substrate surface exhibits a terracing step-shaped fibrous structure, and the size is significantly larger in the range of 10–20 microns; b. the WDE microscopic morphology of the stellite cladding sample shows a honeycomb stalactite peak cluster structure, which is very close to the natural stalactite morphology, and the size of each stalactite petal is about 2 microns. The microstructures may be the underlying reason for determining its superior water droplet erosion resistance.

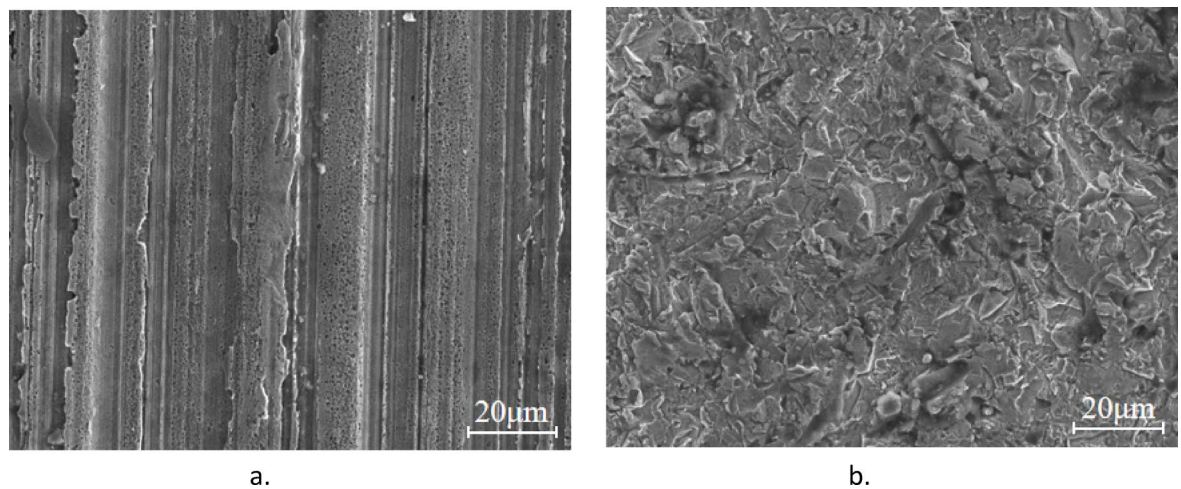


Fig. 22. Surface microstructures of the stellite laser cladding sample. (a) Surface morphology of the wire-cut stellite laser cladding sample; (b) Surface morphology with SPE.

4. The hierarchical honeycomb stalactite clusters in Stellite laser cladding, analogous to millennia-formed natural speleothems, enhance WDE resistance through optimized energy dissipation mechanisms associated with their micron-scale stalactite petal morphology.

The findings enable predictive modeling of multi-phase erosion in turbine blades and oil/gas pipelines by correlating SPE-induced surface topographies with accelerated WDE damage. This indicates the potential advantages of regular textured surfaces for applications in aerospace and wind turbine components exposed to rain and sand erosion.

Data availability

The datasets used and/or analysed during the current study are available from the corresponding author on reasonable request.

Received: 15 December 2024; Accepted: 12 May 2025

Published online: 25 May 2025

References

1. Di, J., Wang, S. S., Yan, X. J., Cai, L. X. & Xie, Y. H. Experimental investigation on effect of surface strengthening process and roughness on water droplet erosion behavior in turbomachinery. *Tribol. Int.* **153**, 106647 (2021).
2. Zhang, Z. Y., Zhang, D. & Xie, Y. H. Experimental study on water droplet erosion resistance of coatings (Ni60 and WC-17Co) sprayed by APS and HVOF. *Wear* **432**, 202950 (2019).
3. Mann, B. Solid-particle erosion and protective layers for steam turbine blading. *Wear* **224**, 8–12 (1999).
4. Di, J., Wang, S.-S., Yan, X.-J., Cai, L.-X. & Xie, Y.-H. Experimental investigation on effect of surface strengthening process and roughness on water droplet erosion behavior in turbomachinery. *Tribol. International* **153**, 106647 (2020).
5. Kirols, H., Kevorkov, D., Uihlein, A. & Medraj, M. The effect of initial surface roughness on water droplet erosion behaviour. *Wear* **342**, 198–209 (2015).
6. Di, J., Wang, S.-S., Jiang, X.-H., Yan, X.-J. & Zhou, W. A Numerical Research on Water Erosion Resistance Characteristics of the Substrate Material of the Last Stage Blades in Steam Turbine. *J. Xi'an Jiaotong Univ.*, 1–9 (2021).
7. Xu, W., Wang, J., Qin, L., Chen, H. & Chen, D. Investigation of erosion damages induced by wet steam containing micro-particles. *Tribol. Lett.* **39**, 115–120 (2010).
8. Wanli, X., Li, Q., Haosheng, C. & Darong, C. Erosion and abrasion on mild carbon steel surface by steam containing SiC microparticles. *Wear* **268**, 1547–1550 (2010).
9. Mahdipoor, M., Tarasi, F., Moreau, C., Dolatabadi, A. & Medraj, M. HVOF sprayed coatings of nano-agglomerated tungsten-carbide/cobalt powders for water droplet erosion application. *Wear* **330**, 338–347 (2015).
10. Mann, B. & Arya, V. An experimental study to correlate water jet impingement erosion resistance and properties of metallic materials and coatings. *Wear* **253**, 650–661 (2002).
11. Ahmad, M., Casey, M. & Sürken, N. Experimental assessment of droplet impact erosion resistance of steam turbine blade materials. *Wear* **267**, 1605–1618 (2009).
12. Hutchings, I. Strain rate effects in microparticle impact. *J. Phys. D Appl. Phys.* **10**, L179 (1977).
13. Evans, A. G., Gulden, M. & Rosenblatt, M. Impact damage in brittle materials in the elastic-plastic response regime. *Proc. R. Soc. London A Math. Phys. Sci.* **361**, 343–365 (1978).
14. Bellman, R. Jr. & Levy, A. Erosion mechanism in ductile metals. *Wear* **70**, 1–27 (1981).
15. Hutchings, I. A model for the erosion of metals by spherical particles at normal incidence. *Wear* **70**, 269–281 (1981).
16. Levy, A. V. The platelet mechanism of erosion of ductile metals. *Wear* **108**, 1–21 (1986).
17. Zhuang, Z. et al. Response characterization on the microstructure, and mechanical and corrosion behavior of clad rebars of different weld materials. *Case Stud. Constr. Mater.* **22**, e04316 (2025).
18. Nekahi, M. M., Vazquez, E. V. & Papini, M. Prediction of the gradual solid particle erosion of particulate-reinforced epoxy-matrix composites using surface evolution modeling. *Tribol. Int.* **193**, 109422 (2024).
19. Lavakumar, B., Padmaganesan, H. T., Prasad, M. & Wasekar, N. P. Enhanced solid particle erosion resistance of nanocrystalline Ni-W coatings through multilayer approach. *Surf. Coat. Technol.* **483**, 130770 (2024).

20. Zhuang, Z. et al. Welding-induced corrosion and protective measures for clad rebars in neutral chloride environments. *Sci. Rep.* **14**, 11657 (2024).
21. Di, J., Wang, S. S. & Xie, Y. H. Investigation on the erosion characteristics of martensitic blade steel material 1Cr12W1MoV by micro-particle swarm with high velocity. *Powder Technol.* **345**, 111–128 (2019).
22. Qin Kefa, F. J. *Theory and Calculation of Engineering Gas-Solid Multiphase Flow* (Zhejiang University Press, 1990).
23. Shen Tianyao, L. J. *Gas-Solid Two-Phase Flow Foundation of Turbomachinery* (China Machine Press, 1994).
24. Tabakoff, W. High-temperature erosion resistance of coatings for use in turbomachinery. *Wear* **186**, 224–229 (1995).
25. Shanov, V. & Tabakoff, W. Erosion resistance of coatings for metal protection at elevated temperatures. *Surf. Coat. Technol.* **86**, 88–93 (1996).
26. Cai, L.-X., Mao, J.-R., Wang, S.-S., Di, J. & Feng, Z.-P. Experimental investigation on erosion resistance of iron boride coatings for steam turbines at high temperatures. *Proc. Instit. Mech. Eng. Part J J. Eng. Tribol.* **229**, 636–645 (2015).
27. Di, J. et al. Experimental research on water droplet erosion resistance characteristics of turbine blade substrate and strengthened layers materials. *Materials* **13**, 4286 (2020).

Acknowledgements

The work was supported by the National Natural Science Foundation of China with Grant No. 52205212, the Fundamental Research Program of Shanxi Province (No. 202203021222206). In addition, the work was also supported by Shanxi Engineering Research Center of Internal Combustion Engine Power Technology and Advanced Technology Innovation Center of Zero Carbon Power Special Vehicle.

Author contributions

Juan DI: Investigation, Writing-Original draft preparation, Experimental Method; Jun JI: Investigation, Experimental testing; Jin XU: SEM electron microscope shooting, Experimental testing; Zhi LI: Data processing, SEM electron microscope shooting; Ke NING: Data processing, Conceptualization; Chao-yi PENG: Supervision, Methodology, Validation; Jian-feng WANG: Supervision, Language Polishing.

Declarations

Competing interests

The authors declare no competing interests.

Additional information

Correspondence and requests for materials should be addressed to J.D.

Reprints and permissions information is available at www.nature.com/reprints.

Publisher's note Springer Nature remains neutral with regard to jurisdictional claims in published maps and institutional affiliations.

Open Access This article is licensed under a Creative Commons Attribution-NonCommercial-NoDerivatives 4.0 International License, which permits any non-commercial use, sharing, distribution and reproduction in any medium or format, as long as you give appropriate credit to the original author(s) and the source, provide a link to the Creative Commons licence, and indicate if you modified the licensed material. You do not have permission under this licence to share adapted material derived from this article or parts of it. The images or other third party material in this article are included in the article's Creative Commons licence, unless indicated otherwise in a credit line to the material. If material is not included in the article's Creative Commons licence and your intended use is not permitted by statutory regulation or exceeds the permitted use, you will need to obtain permission directly from the copyright holder. To view a copy of this licence, visit <http://creativecommons.org/licenses/by-nc-nd/4.0/>.

© The Author(s) 2025